Triple-band antenna using double periodic CRLH resonator on coplanar waveguide

Mohan, Manoj Prabhakar; Alphones, Arokiaswami; Karim, Muhammad Faeyz

ORIGINAL RESEARCH PAPER

Triple-band antenna using double periodic CRLH resonator on coplanar waveguide

Manoj Prabhakar Mohan ⬥ | Arokiaswami Alphones | Muhammed Faeyz Karim

School of Electrical and Electronic Engineering, Nanyang Technological University, Singapore

Correspondence

Arokiaswami Alphones, School of Electrical and Electronic Engineering, Nanyang Technological University, Singapore.
Email: EALPHONES@ntu.edu.sg

Abstract

The uniplanar implementation of double periodic composite right/left-handed (DPCRLH) symmetric unit cell is realized using coplanar waveguide and its analysis with parameter extraction are studied. DPCRLH symmetric unit cell is then experimentally validated. The open-circuited DPCRLH resonator is formed from the DPCRLH unit cell which exhibited five resonance points. The simulated resonant frequencies of the resonator are 1.5494, 2.1968, 3.5072, 5.0438 and 6.089 GHz. A triple-band antenna is designed from the last three resonant frequencies of the resonator. The antenna is horizontally polarized in all three bands. The measured co-polarized gain of the antenna at the central frequencies of the three bands are 1.52 dBi (3.59 GHz), 3.67 dBi (5.1694 GHz) and 1.78 dBi (6.0925 GHz), respectively.

1 | INTRODUCTION

Recently, there has been a rapid development in the future wireless technologies. Because of many specific requirements, the wireless devices need to operate in multiple frequency bands. The multi-band radio frequency circuits including multi-band antennas make the devices compact. Composite right/left-handed (CRLH) has been used in the design of multi-band components due to its non-linear dispersion characteristics and the resonance characteristics of its resonators [1]. Recently, the double periodic composite right/left-handed transmission line (DPCRLH TL) has been paid attention for multi-band applications [2–5]. The unit cell of DPCRLH is formed by concatenating two different unit cells of CRLH TL. It was used in the design of leaky wave antennas to get an additional leaky wave band. The symmetric unit cells of DPCRLH were proposed and analysed in [6]. DPCRLH TL has additional left-handed and right-handed regions compared to conventional CRLH TL. The design of open-circuited DPCRLH resonator and the design of triple-band filter using DPCRLH resonator were reported in [7].

The uniplanar implementation of CRLH unit cell using coplanar waveguide (CPW) has been implemented in [8] and its parameter extraction based on effective medium theory was also reported. In [9], the design of CRLH resonator at zeroth-order resonance and the design of bandpass filter with

spurious suppression were experimentally verified. The design of various filters using CRLH short-circuited stubs was reported in [10–12].

Two dual-band antennas using CRLH TL with novel terminations to operate at zeroth-order series and shunt resonances were designed in [13]. Symmetric, asymmetric, and chip-loaded CRLH zeroth-ordered resonant (ZOR) antennas were reported in [14]. A wideband antenna obtained by combining zeroth-order and first-order resonances of CRLH TL in asymmetric CPW was reported in [15]. The same principle was used in the design of epsilon negative wideband antenna in CPW [16]. The epsilon negative dual-band and wideband antennas using ZOR and first-order resonance were designed in [17]. The epsilon negative and double negative meta-structured transmission lines were used to design ZOR antennas in [18]. Both the antennas have the same radiation characteristics. A short-circuited wideband CPW ZOR antenna was reported in [19]. All the above antennas were designed for dual-band or wideband applications. CRLH unit cell was loaded to rectangular loop to form triple-band antenna in [20]. Here the resonant frequencies depend on the length of the rectangular loop. A triple-band antenna using CRLH resonant structures was reported in [21]. There is no description about control of resonant frequencies and bandwidths of the antenna. A triple antenna was designed in [22] using CRLH

unit-cell-loaded monopole antenna. Here also the resonant frequencies depend on the length of the monopole.

In this work, the uniplanar implementation of the DPCRLH symmetric unit cell in CPW configuration is studied. Further, the design of DPCRLH open-circuited resonator and design of triple-band antenna using DPCRLH open-circuited resonator are discussed. The design of the DPCRLH symmetric unit cell and its parameter extraction are given in Section 2. The design of open-circuited resonator and analysis of triple-band antenna are given in Sections 3 and 4, respectively.

2 | DESIGN OF DPCRLH SYMMETRIC UNIT CELL

The symmetric unit cells of DPCRLH are introduced in [6]. In this paper, the symmetric unit cell shown in Figure 1 is implemented in CPW. The impedance and the admittance parameters of DPCRLH unit cell in Figure 1 are given as follows:

$$Z_1 = j\omega L_{R1} + \frac{1}{j\omega C_{L1}} \qquad (1)$$

$$Z_2 = j\omega L_{R2} + \frac{1}{j\omega C_{L2}} \qquad (2)$$

$$Y_1 = j\omega C_{R1} + \frac{1}{j\omega L_{L1}} \qquad (3)$$

The ABCD matrix and the detailed analysis of dispersion diagram of the unit cell in Figure 1 are given in [6], and the parameter values of ABCD matrix are

$$A = D = 1 + Z_1 Y_1 + Z_1 Y_2 + \frac{Z_1^2 Y_1 Y_2}{2} \qquad (4)$$

$$B = 2Z_1 + Z_1^2 Y_1 \qquad (5)$$

$$c = Y_1 + Y_2 + Z_1 Y_1 Y_2 + \frac{Z_1 Y_2^2}{2} + \frac{Z_1^2 Y_1 Y_2^2}{4} \qquad (6)$$

The propagation constant is given as $\cosh \gamma d = \frac{A+D}{2}$ [23]. In the lossless case, within the pass band, the phase constant becomes $\cos \beta d = \frac{A+D}{2}$. For the unit cell in Figure 1, the phase constant is given as

$$\cos \beta d = \frac{A+D}{2} = 1 + Z_1 Y_1 + Z_1 Y_2 + \frac{Z_1^2 Y_1 Y_2}{2} \qquad (7)$$

The dispersion diagram of the DPCRLH is shown in Figure 2. The $\beta d = 0$ and $\beta d = \pi$ frequency points are plotted in Figure 2. The expressions for these frequency points in the dispersion diagram are found out by substituting $\beta d = 0$ and $\beta d = \pi$ in Equation (7). At $\beta d = 0$, Equation (7) becomes

$$Z_1 Y_1 + Z_1 Y_2 + \frac{Z_1^2 Y_1 Y_2}{2} = 0 \qquad (8)$$

The solutions of Equation (8) are found out as

$$Z_1 = 0 \ \& \ Y_1 + Y_2 + \frac{Z_1 Y_1 Y_2}{2} = 0 \qquad (9)$$

At $\beta d = \pi$, Equation (7) becomes

$$Z_1 Y_1 + Z_1 Y_2 + \frac{Z_1^2 Y_1 Y_2}{2} = -2 \qquad (10)$$
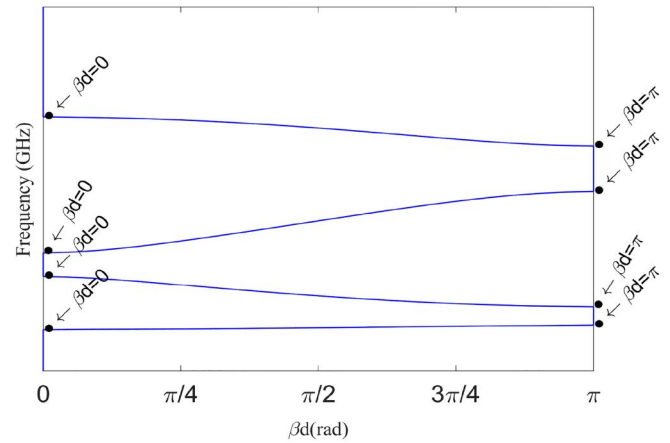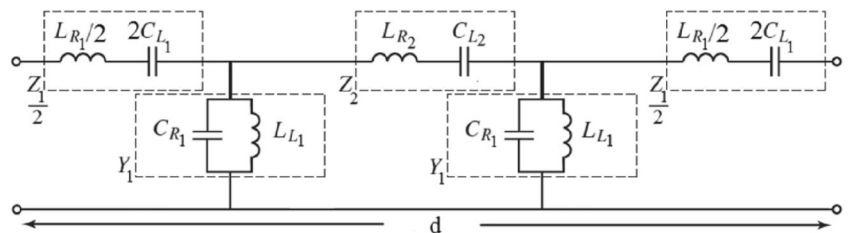
The solutions of Equation (10) are

FIGURE 2 Dispersion diagram of a double periodic composite right/left-handed unit cell

FIGURE 1 Symmetric unit cell of double periodic composite right/left-handed transmission line

$$Z_1Y_1 = -2 \;\&\; Z_1Y_2 = -2 \qquad (11)$$

From the ABCD parameters of the unit cell, Y_{21} can be found out using the relation given in [23] as

$$Y_{21} = Y_{12} = \frac{-1}{2Z_1 + Z_1^2 Y_1} = \frac{-1}{Z_1(2 + Z_1 Y_1)} \qquad (12)$$

From Equation (12), ideally Y_{21} becomes infinite at $Z_1 = 0$ and $(2 + Z_1 Y_1) = 0$. $Z_1 = 0$ is one of the four $\beta d = 0$ points in the dispersion diagram (from Equation [9]). $(2 + Z_1 Y_1) = 0$ is two of the four $\beta d = \pi$ points (from Equation [11]). The parameter Z_{21} is obtained from the ABCD parameters by using the relation in [23]. It is given as

$$Z_{21} = Z_{12} = \frac{1}{(Z_1 Y_2 + 2)\left(Y_1 + Y_2 + \frac{Z_1 Y_1 Y_2}{2}\right)} \qquad (13)$$

Ideally, Z_{21} becomes infinite at $Z_1 Y_2 + 2 = 0$ and $Y_1 + Y_2 + \frac{Z_1 Y_1 Y_2}{2} = 0$. The equations $Z_1 Y_2 + 2 = 0$ and $Y_1 + Y_2 + \frac{Z_1 Y_1 Y_2}{2} = 0$ represent the remaining two $\beta d = \pi$ points and three $\beta d = 0$ points in the dispersion diagram, respectively.

$Z_1 Y_1 = -2$ in Equation (11) can be simplified as

$$L_{L1}C_{R1} - \frac{1}{\omega^2}\left(1 + \frac{C_{R1}L_{L1}}{L_{R1}C_{L1}} + \frac{2L_{L1}}{L_{R1}}\right) + \frac{1}{\omega^4 C_{L1}L_{R1}} = 0 \qquad (14)$$

Substituting $L_{L1}C_{R1} = a_1 \;\frac{L_{L1}}{L_{R1}} = b_1$ in Equation (14) gives

$$a_1 - \frac{1}{\omega^2}\left(1 + \frac{a_1}{L_{R1}C_{L1}} + 2b_1\right) + \frac{1}{\omega^4 C_{L1}L_{R1}} = 0 \qquad (15)$$

$Z_1 Y_1 = -2$ contains twos of the four $\beta d = \pi$ points; so Equation (15) is satisfied at two frequency points $\omega = \omega_{\pi 1}$ and $\omega = \omega_{\pi 2}$. $Z_1 = 0$ is one of the $\beta d = 0$ points, which occurs at $\omega_0^2 = \frac{1}{L_{R1}C_{L1}}$. So, Equation (15) can be written in the form of two equations given as

$$a_1 - \frac{1}{\omega_{\pi 1}{}^2}\left(1 + a_1\omega_0^2 + 2b_1\right) + \frac{\omega_0^2}{\omega_{\pi 1}{}^4} = 0 \qquad (16)$$

$$a_1 - \frac{1}{\omega_{\pi 2}{}^2}\left(1 + a_1\omega_0^2 + 2b_1\right) + \frac{\omega_0^2}{\omega_{\pi 2}{}^4} = 0 \qquad (17)$$

Similarly, another two equations can be obtained from $Z_1 Y_2 = -2$ of Equation (11). They are

$$a_2 - \frac{1}{\omega_{\pi 3}{}^2}\left(1 + a_2\omega_0^2 + 2b_2\right) + \frac{\omega_0^2}{\omega_{\pi 3}{}^4} = 0 \qquad (18)$$

$$a_2 - \frac{1}{\omega_{\pi 4}{}^2}\left(1 + a_2\omega_0^2 + 2b_2\right) + \frac{\omega_0^2}{\omega_{\pi 4}{}^4} = 0 \qquad (19)$$

where $a_2 = L_{L2}C_{R2}$, $b_2 = \frac{L_{L2}}{L_{R1}}$, and $\omega = \omega_{\pi 3}$ $\omega = \omega_{\pi 4}$ are the remaining two $\beta d = \pi$ points.

The interdigital capacitor and short-circuited stub are used to achieve the left-handed properties in the DPCRLH unit cell. The value of L_{L1} is found out by simulating the short-circuit stub alone and comparing the simulated Z parameters with Z parameters of the equivalent circuit of the short-circuited stub. L_{L1} can be given as

$$L_{L1} = \frac{2j}{\omega}\left[\omega\frac{\partial\left(\frac{1}{Z_{21}^{sc}}\right)}{\partial\omega} - \frac{1}{Z_{21}^{sc}}\right]^{-1} \qquad (20)$$

where Z_{21}^{sc} is the simulated Z_{21} of the short-circuited stub and ω is the frequency at which L_{L1} is extracted. The other parameters of the DPCRLH unit cell are found out by solving Equations (16)–(19). Based on the above analysis, a DPCRLH unit cell in CPW is designed and it is shown in Figure 3 along with the simulated Y_{21} and Z_{21} parameters. CST Microwave studio is used for all the simulations in this work. The substrate used is Rogers R04003C with dielectric constant of 3.55, loss tangent of 0.0027, and thickness of 1.524 mm. L_{L1} is found out by simulating the short-circuited stub separately, and it is found out as 3.197 nH. The frequencies $\omega_{\pi 1}$–$\omega_{\pi 4}$ are found out from the simulated Y_{21} and Z_{21}. Substituting $\omega_{\pi 1}$–$\omega_{\pi 4}$ in Equations (16)–(19) and solving them gives the parameter values of DPCRLH unit cell. The parameter values of DPCRLH unit cell are found out as $L_{R1} = 4$ nH, $C_{L1} = 0.72$ pF, $L_{L1} = 3.197$ nH, $C_{R1} = 0.79$ pF, $L_{L2} = 1.04$ nH, and $C_{R2} = 1.15$ pF. The photograph of the fabricated filter along with the simulated and measured S parameters and dispersion diagram are shown in Figure 4. The simulated and measured S-parameter responses match quite well. The propagation constant extracted from the simulated and measured S parameters are compared with the propagation constant obtained by substituting DPCRLH unit cell parameters in Equation (7) and shown in Figure 4(c).

3 | DPCRLH RESONATOR

After analysing the unit cell, DPCRLH resonator is formed by introducing open circuits at both ends of the resonator. The input impedance of the open-circuited DPCRLH resonator is given in [6] as
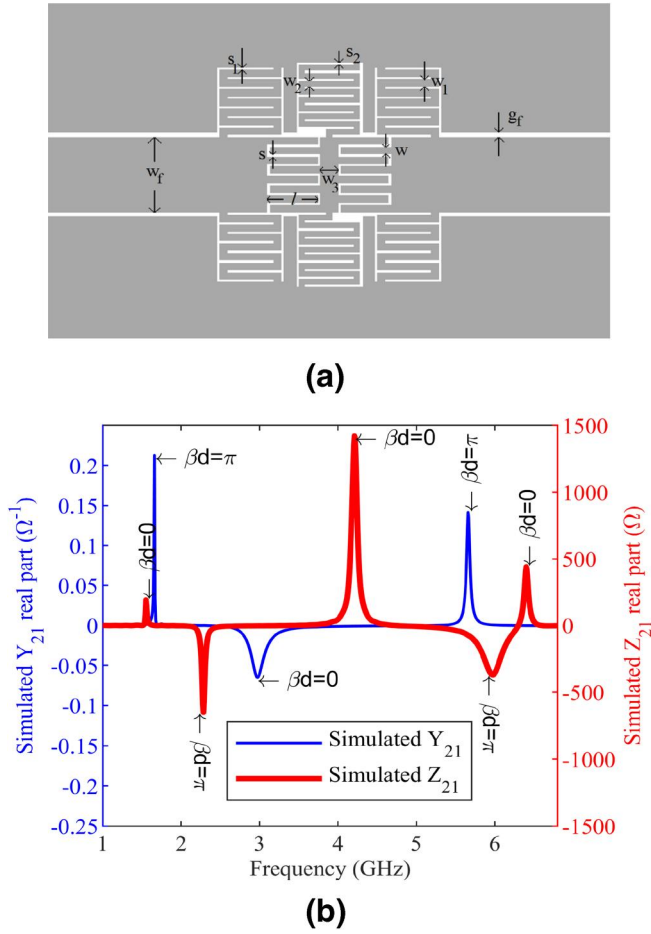
(a)

(b)

FIGURE 3 (a) Structure of DPCRLH unit cell with $l = 3$ mm, $w = 0.4$ mm, $w_1 = 0.4$ mm, $w_2 = 0.3$ mm, $w_3 = 1$ mm, $s = s_1 = s_2 = 0.2$ mm, $w_f = 4.6$ mm, and $g_f = 0.33$ mm. (b) Simulated real parts of Y_{21} and Z_{21}

$$Z_{in} = \frac{2\left(Z_1^2 Y_1 Y_2 + 2Z_1 Y_2 + 2Z_1 Y_1 + 2\right)}{4\left(Y_1 + Y_2 + \frac{Z_1 Y_1 Y_2}{2}\right)(Z_1 Y_2 + 2)} \quad (21)$$

At resonance,

$$4\left(Y_1 + Y_2 + \frac{Z_1 Y_1 Y_2}{2}\right)(Z_1 Y_2 + 2) = 0 \quad (22)$$

DPCRLH unit cell parameters $L_{R1} = 4$ nH, $C_{L1} = 0.72$ pF, $L_{L1} = 3.197$ nH, $C_{R1} = 0.79$ pF, $L_{L2} = 1.04$ nH, and $C_{R2} = 1.15$ pF are substituted in Equation (21), and the resonance frequencies are 1.54, 2.28, 4.02, 5.98, and 6.97 GHz. The DPCRLH open-circuited resonator is shown in Figure 5 along with the simulated S parameters. The simulated resonance frequencies are 1.5494, 2.1968, 3.5072, 5.0438, and 6.089 GHz.

If the resonator is assumed to be lossless, then the external quality factor is given as [24, 25]
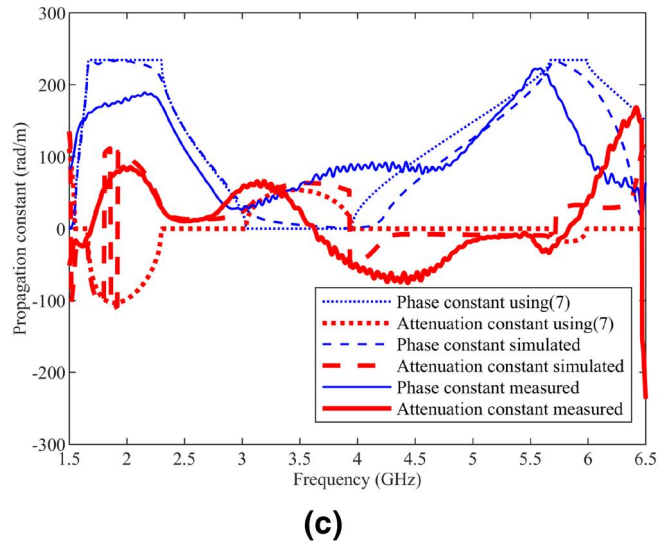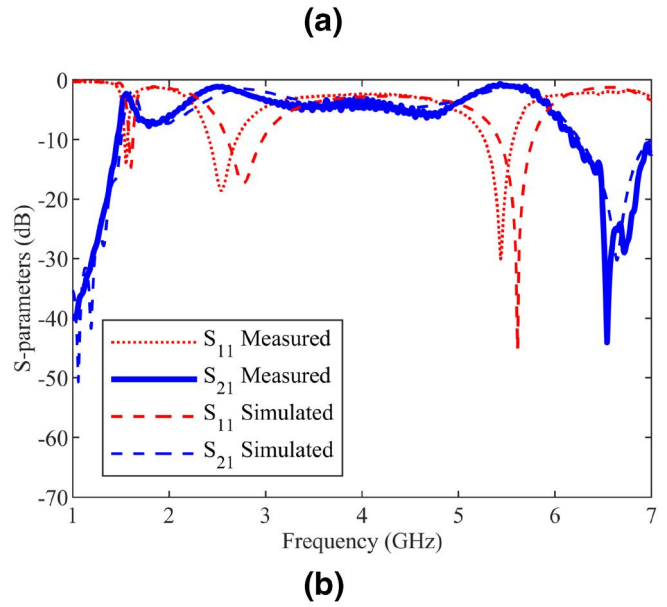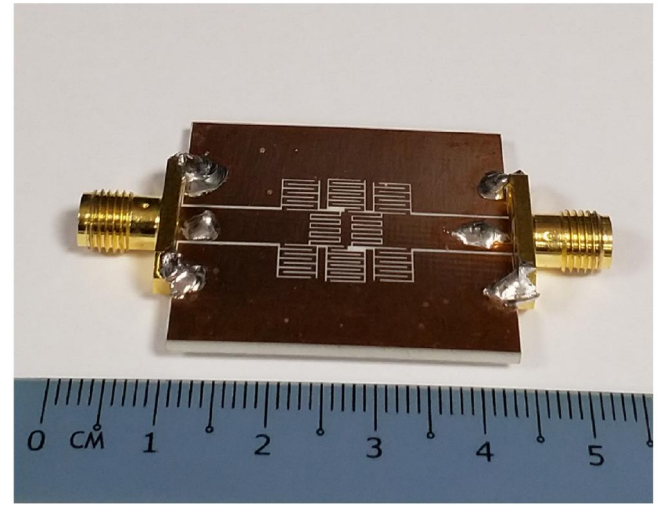

(a)

(b)

(c)

FIGURE 4 (a) Photograph of the fabricated double periodic composite right/left-handed unit cell. (b) Simulated and measured S-parameter responses. (c) Dispersion diagram
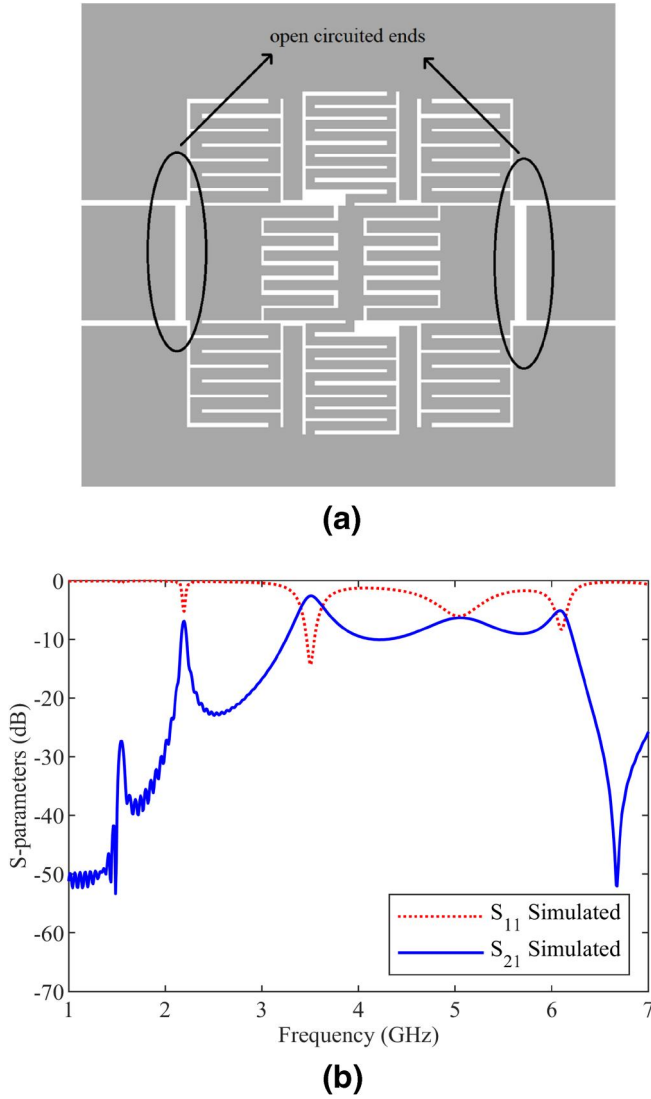
(a)

(b)

FIGURE 5 Double periodic composite right/left-handed (DPCRLH) open-circuited resonator: (a) DPCRLH resonator structure; (b) Simulated S-parameter responses

$$Q = \frac{\omega}{2G}\frac{\partial B}{\partial \omega} \qquad (23)$$

where G is the shunt conductance at the terminal of the resonator and B is the susceptance of the resonator. The quality factor at resonant frequency points is important. The susceptance of the resonator is given as

$$B = \frac{1}{j}\frac{4\left(Y_1 + Y_2 + \frac{Z_1 Y_1 Y_2}{2}\right)(Z_1 Y_2 + 2)}{2\left(Z_1^2 Y_1 Y_2 + 2Z_1 Y_2 + 2Z_1 Y_1 + 2\right)} \qquad (24)$$

From Equation (24), $\frac{\partial B}{\partial \omega}$ at $(Z_1 Y_2 + 2) = 0$ resonant points can be found out as

$$\frac{\partial B}{\partial \omega} = \frac{1}{2j}\left(2Y_2' - Z_1' Y_2^2\right) \qquad (25)$$

where Y_2' and Z_1' are the derivatives of Y_2 and Z_1. The external quality factor at $(Z_1 Y_2 + 2) = 0$ resonant points is found out from Equations (23) and (25) as

$$Q = \frac{\omega}{4jG}\left(2Y_2' - Z_1' Y_2^2\right) \qquad (26)$$

From Equation (26), it can be concluded that, if the values of L_{R1} and C_{R2} are decreased and the values of C_{L1} and L_{L2} are increased, the bandwidth will increase at the two resonant points given by $(Z_1 Y_2 + 2) = 0$. $\frac{\partial B}{\partial \omega}$ at $(Y_1 + Y_2 + \frac{Z_1 Y_1 Y_2}{2}) = 0$ resonant points, which is derived from Equation (24) as

$$\frac{\partial B}{\partial \omega} = \frac{1}{2j}\left(2Y_2' - Z_1' Y_2^2 + \frac{Y_1'}{2}(2 + Z_1 Y_2)^2\right) \qquad (27)$$

where Y_2', Z_1', and Y_1' are the derivatives of Y_2, Z_1, and Y_2. The external quality factor at the remaining three $(Y_1 + Y_2 + \frac{Z_1 Y_1 Y_2}{2}) = 0$ resonant points is found out from Equations (23) and (27) as

$$Q = \frac{\omega}{4jG}\left(2Y_2' - Z_1' Y_2^2 + \frac{Y_1'}{2}(2 + Z_1 Y_2)^2\right) \qquad (28)$$

From Equation (28), it can be found out, if the values of L_{R1}, C_{R1}, and C_{R2} are decreased and the values of C_{L1}, L_{L1}, and L_{L2} are increased, the bandwidth will increase at three resonant points given by $(Y_1 + Y_2 + \frac{Z_1 Y_1 Y_2}{2}) = 0$. Also, comparing Equations (26) and (28), Equation (28) has one extra term, so bandwidth at $(Z_1 Y_2 + 2) = 0$ resonant point is always higher than bandwidth at $(Y_1 + Y_2 + \frac{Z_1 Y_1 Y_2}{2}) = 0$ resonant points.

4 | DESIGN OF TRIPLE BAND ANTENNA

The triple-band antenna is formed from the last three resonant frequencies of the DPCRLH open-circuited resonator. The antenna is matched at the three frequencies by introducing the discontinuities in the feed line. The ground planes on both sides of CPW are extended up to 22.37 mm. The structure of the antenna and its photograph and the simulated and measured S-parameter responses are shown in Figure 6. The reason for the frequency shift between the simulated and measured results is due to the fabrications errors. The measured central frequencies of the antenna are 3.59, 5.1694, and 6.0925 GHz, whereas the simulated central frequencies are
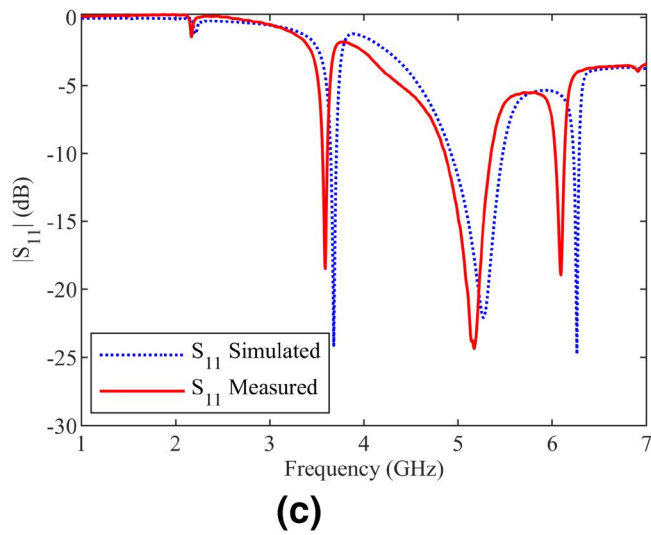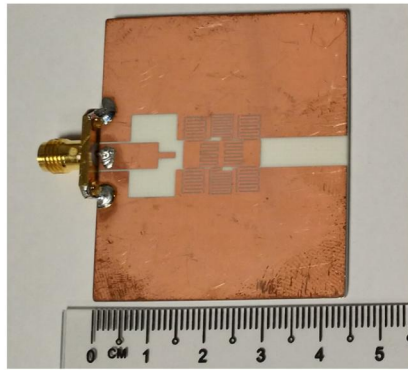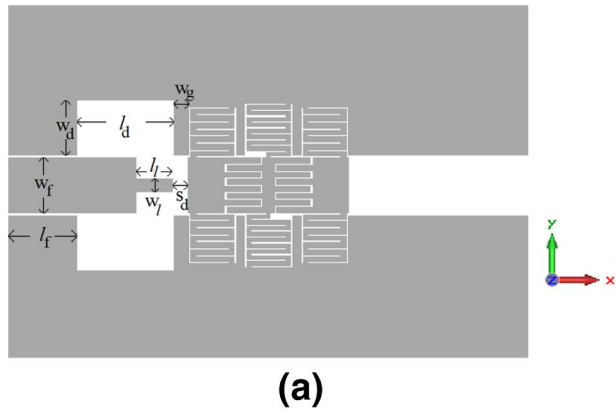
(a)

(b)

(c)

FIGURE 6 Coplanar waveguide double periodic composite right/left-handed triple-band antenna: (a) structure of the antenna with $w_f = 4.6$ mm, $l_f = 5.6$ mm, $w_d = 5$ mm, $l_d = 8.2$ mm, $s_d = 1.4$ mm, $w_l = 1$ mm, $l_l = 3$ mm, and $w_g = 1.2$ mm. (b) Photograph of the fabricated antenna. (c) Simulated and measured S-parameter responses

(a)

(b)

(c)

FIGURE 7 Simulated and measured radiation patterns of antenna in XZ plane (E plane) at the central frequencies of (a) first band, (b) second band, and (c) third band

3.6788, 5.27, and 6.2606 GHz. The measured 10 dB bandwidth at the three bands are 1.52%, 9.48%, and 1.78%. The bandwidths are in accordance with Equations (26) and (28). The first and last bands have approximately equal bandwidths
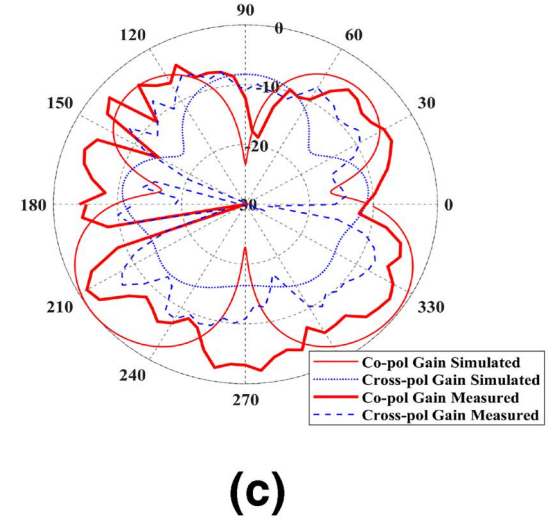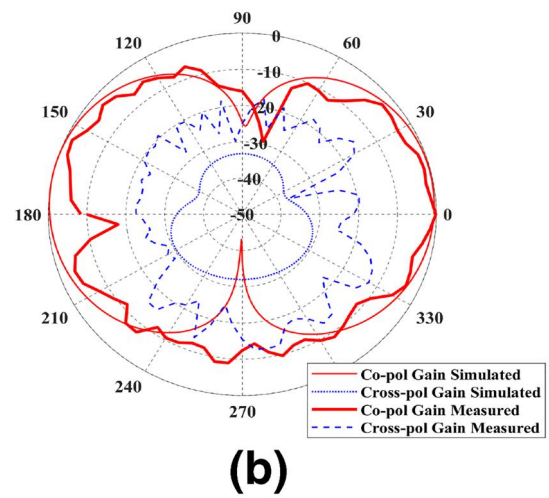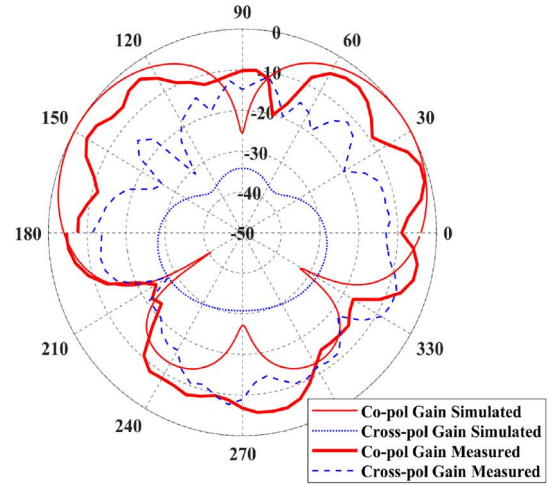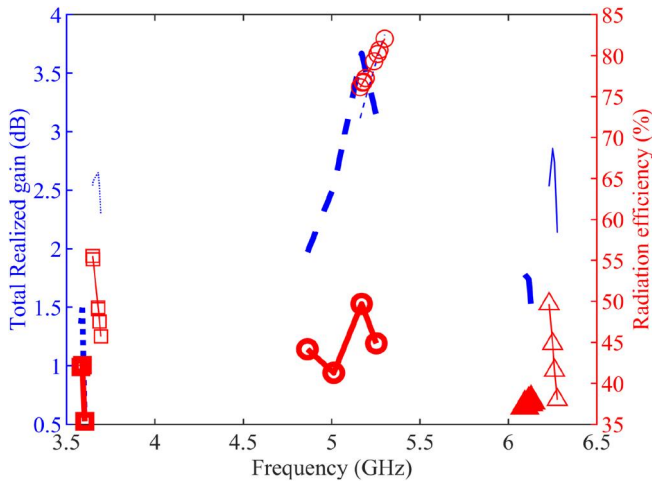
FIGURE 8 Simulated total realized gain and simulated radiation efficiency versus frequency. The simulated results are shown in thin lines and the measured results are shown in thick lines. The realized gains in the first, second, and third bands are represented by dotted, dashed, and solid lines, respectively. The radiation efficiencies in the first, second, and third bands are represented by lines with square, circle, and triangle marker symbols, respectively

$((Y_1 + Y_2 + \frac{Z_1 Y_1 Y_2}{2}) = 0$ resonant points), and they have lower bandwidth than the second band $((Z_1 Y_2 + 2) = 0$ resonant point). The simulated and measured radiation pattern of the antenna in the XZ $(\Phi = 0)$ plane for the three bands are shown in Figure 7. The antenna is horizontally polarized in all the three bands. The measured co-polarization gain of the antenna at the central frequencies of the three bands are 1.52 dBi (3.59 GHz), 3.67 dBi (5.1694 GHz), and 1.78 dBi (6.0925 GHz). The simulated co-polarization gain of the antenna in three bands are 2.648 dBi (3.6788 GHz), 3.695 dBi (5.27 GHz), and 2.66 dBi (6.2606 GHz). The measured radiation efficiencies are 42.24% (3.59 GHz), 49.69% (5.1694 GHz), and 37.22% (6.0925 GHz), whereas the simulated radiation efficiencies are 49.28% (3.6788 GHz), 80.69% (5.27 GHz), and 41.57% (6.2606 GHz) at the central frequencies of three bands. The connector of the antenna makes the nulls at 270° in the measured radiation patterns of the three bands to disappear. The connector is of comparable size to the radiating part of the antenna and it reflects the waves during measurement. It is also evident from Figure 7, the nulls at 90° in the measured radiation patterns of three bands are not affected because of the absence of the connector there.

TABLE 1 Comparison of the designed triple-band antenna with that of existing works

	Frequency (GHz) and number of bands	Antenna footprint λ_0	Bandwidth %	Gain (dBi)	Radiation efficiency %	Layer
This work	Triple-band antenna 3.59, 5.1694, and 6.0925	0.519 × 0.60 (Including ground planes)	1.47, 9.48, and 1.58	1.52, 3.67, and 1.78	42.24, 49.69, and 37.22	Single
[12]	Two dual-band antennas	0.113 × 0.135 ($f_{se} < f_{sh}$)	0.6 and 1.7 ($f_{se} < f_{sh}$)	1.08 and 1.12 ($f_{se} < f_{sh}$)	62 and 65 ($f_{se} < f_{sh}$)	Single
	2.33 and 2.87 ($f_{se} < f_{sh}$) 2.41 and 3.04 ($f_{se} > f_{sh}$)	0.111 × 0.126 ($f_{se} > f_{sh}$)	1.2 and 0.2 ($f_{se} > f_{sh}$)	1.47 and −1.71 ($f_{se} > f_{sh}$)	63 and 60 ($f_{se} > f_{sh}$)	
[13]	Two single wideband antennas	0.097 × 0.053 (symmetric)	6.8 (symmetric)	1.35 (symmetric)	62 (symmetric)	Double
	2.03 (symmetric), 1.5 (asymmetric)	0.072 × 0.04 (asymmetric)	4.8 (asymmetric)	−2.15 (asymmetric)	42.5 (asymmetric)	
[14]	Wideband antenna 1.77 to 3.77	0.049 × 0.136	58.1	1.6 at ZOR, and 3.25 at FOR	73.3 at ZOR 74.5 at FOR	Single
[16]	Dual band antenna 1.88 (ZOR) and 3.22 (FOR)	0.031 × 0.089	15.79 (ZOR) 29.03 (FOR)	1.94 (ZOR) 2.95 (FOR)	92.09 (ZOR) 88.02 (FOR)	Double
[18]	Single wideband antenna 2.16	0.14 × 0.22	15.1	1.62	72	Single
[20]	Triple-band antenna 2.37–2.64, 3.39–3.58, 4.86–6.98	0.21 × 0.38	10.8, 5.4, 38.3	−2, 0.14, 3.2	More than 90 in all the bands	Double
[21]	Triple-band antenna 1.78, 4.22, 5.8	0.11 × 0.11	3.08, 15.17, 8.33	−0.15, ~3.5, 3–3.5	70, >80, >90 (simulated efficiencies)	Single
[22]	Triple-band antenna 0.925, 1.227, 2.1	0.29 × 0.17	8.65, 3.26, 54.29 (all are 6 dB bandwidths)	Not given	92, 76, 99 (simulated efficiencies)	Double

Abbreviations: FOR, first-ordered resonant; ZOR, zeroth-ordered resonant.

Also, the connector increased the cross-polarization component to a small amount around $270°$ in the measured radiation patterns. The variation of simulated and measured total realized gains and radiation efficiencies with respect to the frequency are shown in Figure 8. The comparison of the designed triple-band antenna with other CPW-based metamaterial antennas is given in Table 1.

5 | CONCLUSION

The uniplanar DPCRLH symmetric unit cell has been implemented in CPW. The parametric extraction and the analysis of the DPCRLH unit cell have been studied first and is experimentally validated. The design of the open-circuited DPCRLH resonator from the DPCRLH unit cell is discussed. DPCRLH resonator has five resonance points. The triple-band antenna is formed by the last three resonant frequencies of DPCRLH resonator. The triple-band antenna has the measured co-polarization gain in the three bands as 1.52 dBi (3.59 GHz), 3.67 dBi (5.1694 GHz), and 1.78 dBi (6.0925 GHz). Thus, uniplanar DPCRLH unit cell can be implemented and its resonator can be used in the design of multi-band components.

ORCID

Manoj Prabhakar Mohan https://orcid.org/0000-0002-8825-4990

REFERENCES

1. Caloz, C., Itoh, T.: Electromagnetic Metamaterial: Transmission Line Theory and Microwave Applications. Wiley (2005)
2. Jin, C., Alphones, A., Tsutsumi, M.: Double periodic composite right/left handed transmission line and its applications to compact leaky-wave antennas. IEEE Trans. Antenn. Propag. 59(10), 3679–3686 (2011)
3. Jin, C., Alphones, A.: Leaky-wave radiation behavior from a double periodic composite right/left-handed substrate integrated waveguide. IEEE Trans. Antenn. Propag. 60(4), 1727–1735 (2012)
4. Jin, C., Alphones, A.: Double periodic composite right/left handed substrate integrated waveguide. In: Asia-Pacific Microwave Conference 2011, Melbourne, VIC, pp. 429–432 (2011)
5. Jin, C., Alphones, A., Tsutsumi, M.: Leaky-wave characteristics from double periodic composite right-/left-handed transmission lines. IET Microw. Antenn. Propag. 5(12), 1399–1407 (2011)
6. Mohan, M.P., Alphones, A.: Double periodic CRLH transmission line for wideband performance. In: 2016 Asia-Pacific Microwave Conference (APMC), New Delhi, pp. 1–4 (2016)
7. Mohan, M.P., Alphones, A., Karim, M.F.: Triple band filter based on double periodic CRLH resonator. IEEE Microw. Wirel. Compon. Lett. 28(3), 212–214 (2018)
8. Mao, S.-G., Wu, M.-S.: Equivalent circuit modeling of symmetric composite right/left-handed coplanar waveguides. In: IEEE MTT-S International Microwave Symposium Digest, Long Beach, CA, pp. 1953–1956 (2005)
9. Mao, S.-G., et al.: Modeling of symmetric composite right/left-handed coplanar waveguides with applications to compact bandpass filters. IEEE Trans. Microw. Theor. Tech. 53(11), 3460–3466 (2005)
10. Mao, S., Wu, M.: Compact composite right/left-handed coplanar waveguide filters with arbitrary passband and stopband responses. In: 2006 IEEE MTT-S International Microwave Symposium Digest, San Francisco, CA, pp. 369–372 (2006)
11. Mao, S., Wu, M., Chueh, Y.: Design of composite right/left-handed coplanar-waveguide bandpass and dual-passband filters. IEEE Trans. Microw. Theo.r Tech. 54(9), 3543–3549 (2006)
12. Mao, S., Chueh, Y., Wu, M.: Asymmetric dual-passband coplanar waveguide filters using periodic composite right/left-handed and quarter-wavelength stubs. IEEE Microw. Wirel. Compon. Lett. 17(6), 418–420 (2007)
13. Chiu, S., Lai, C., Chen, S.: Compact CRLH CPW antennas using novel termination circuits for dual-band operation at zeroth-order series and shunt resonances. IEEE Trans. Antenn. Propag. 61(3), 1071–1080 (2013)
14. Jang, T., Choi, J., Lim, S.: Compact coplanar waveguide (CPW)-fed zeroth-order resonant antennas with extended bandwidth and high efficiency on vialess single layer. IEEE Trans. Antenn. Propag. 59(2), 363–372 (2011)
15. Niu, B., Feng, Q.: Bandwidth enhancement of asymmetric coplanar waveguide (ACPW)-fed antenna based on composite right/left-handed transmission line. IEEE Antenn. Wirel. Propag. Lett. 12, 563–566 (2013)
16. Niu, B., Feng, Q.: Bandwidth enhancement of CPW-fed antenna based on epsilon negative zeroth- and first-order resonators. IEEE Antenn. Wirel. Propag. Lett. 12, 1125–1128 (2013)
17. Niu, B.J., Feng, Q.Y., Shu, P.L.: Epsilon negative zeroth- and first-order resonant antennas with extended bandwidth and high efficiency. IEEE Trans. Antenn. Propag. 61(12), 5878–5884 (2013)
18. Park, J., et al.: Epsilon negative zeroth-order resonator antenna. IEEE Trans. Antenn. Propag. 55(12), 3710–3712 (2007)
19. Chi, P., Shih, Y.: Compact and bandwidth-enhanced zeroth-order resonant antenna. IEEE Antenn. Wirel. Propag. Lett. 14, 285–288 (2015)
20. Nandi, S., Mohan, A.: CRLH unit cell loaded triband compact MIMO antenna for WLAN/WiMAX applications. IEEE Antenn. Wirel. Propag. Lett. 16, 1816–1819 (2017)
21. Amani, N., et al.: Compact tri-band metamaterial-inspired antenna based on CRLH resonant structures. Electron. Lett. 50(12), 847–848 (2014)
22. Ibrahim, A.A., Safwat, A.M.E., El-Hennawy, H.: Triple-band microstrip-fed monopole antenna loaded with CRLH unit cell. IEEE Antenn. Wirel. Propag. Lett. 10, 1547–1550 (2011)
23. Pozar, D. M.: Microwave Engineering, 4th ed. Wiley, Hoboken, NJ (2012)
24. Harrington, R. F.: Time-Harmonic Electromagnetic Fields (McGraw-Hill Texts in Electrical Engineering). McGraw-Hill, New York (1961)
25. Montgomery, C.G., Dicke, R.H., Purcell, E.M. (eds.).: Principles of Microwave Circuits. Institution of Engineering and Technology (1987)